



CHORUS

This is the accepted manuscript made available via CHORUS. The article has been published as:

High-resistance state of phase coherent nanoscale thin-film Al superconducting nanorings in magnetic fields

S. D. Snyder, T. Dunn, M. J. Erickson, J. Kinney, Yeonbae Lee, J. Nelson, and A. M Goldman

Phys. Rev. B **87**, 144503 — Published 3 April 2013

DOI: [10.1103/PhysRevB.87.144503](https://doi.org/10.1103/PhysRevB.87.144503)

High-Resistance State of Phase Coherent Nanoscale Thin-Film Al Superconducting Nanorings in Magnetic Fields

S. D. Snyder, T. Dunn, M. J. Erickson, J. Kinney, Yeonbae Lee, J. Nelson and A. M Goldman
School of Physics and Astronomy, University of Minnesota, Minneapolis, MN 55455, USA

An interesting and novel effect has been observed in the form of a high resistance state below the superconducting transition temperature of Al nanorings. The resistance exceeded fifteen times the value of the normal state resistance even though the ring was superconducting. This counterintuitive effect can be explained in terms of charge imbalance caused by the nonequilibrium accumulation of quasiparticles near tilted normal-superconductor interfaces that occur naturally in highly constricted nanostructures. Simulations using finite element analysis have been performed which support the experimental results. Similar results have been observed in wires and disks, but the results of this work clarify and extend this previous work.

PACS numbers: PACS number

I. INTRODUCTION

The nature of the physics of superconducting structures smaller than the spatial extent of Cooper pairs is an interesting question that has been investigated for some time. Many interesting physical effects have been observed in dimensionally constrained superconductors including, but not limited to: superconductor-insulator transitions,¹ resistance anomalies,² thermal and quantum fluctuation effects^{3,4} and field induced stabilization of superconductivity.⁵ It has even been suggested that superconducting nanowires could be used as qubits.⁶ While much progress has been made, open questions still abound.

For example it was predicted that the well known Little-Parks effect (LPE)⁷ in superconducting rings would change in period from $h/2e$ to h/e in rings with dimensions smaller than the coherence length, ξ_0 , a measure of the Cooper pair size.⁸⁻¹⁰ This effect had not been observed experimentally, motivating the present work.

This limit is also associated with the destructive regime,^{11,12} which can be suppressed by adding probes to the rings.¹³ To avoid the destructive regime, in which the transition temperature is suppressed to zero at a threading flux of $h/2e$, a four-probe geometry was used. Similar geometries have been employed in microscopic superconducting rings, and the LPE has been observed.¹⁴ However on the nanoscale what occurs is substantially different.

This work will demonstrate a *phase coherent* high resistance state (HRS) observed in magnetic field with the resistance exceeding fifteen times the normal state value. This is the first measurement of such an HRS in nanorings. Previous observations of a phase coherent HRS have

been made in disks, but a solid understanding hasn't been achieved.¹⁵⁻¹⁹ However, through the experiments and simulations presented here, this phenomenon can now be understood as the manifestation of tilted normal metal - superconducting (NS) boundaries which arise naturally in these nanostructures.²

II. EXPERIMENTAL RESULTS

The samples were made using a standard mix and match of lithography and liftoff techniques. Ti/Au contacts were pre-fabricated on SiO₂ thermally coated *p*-doped Si wafers. The samples were then written in 200nm thick PMMA using a Vistec EBPG 5000+ e-beam lithography tool. Two of the designs used will be discussed here (Fig. 1(a) shows the first geometry). The Al films were deposited in a UHV e-beam evaporator at pressures $\lesssim 1 \times 10^{-8}$ Torr and deposition rates ~ 3 Å/s at room temperature to a thickness of ~ 30 nm. They were then transferred as quickly as possible to an Oxford Instruments Kelvinox 25 dilution refrigerator with a base temperature of 80mK equipped with a 12T magnet. Measurements of resistance were made using a Keithley 2182A voltmeter and a 6221 current source. The ξ_0 was ~ 110 nm as measured by standard techniques.¹¹ Disorder in the granular liftoff structures limited ξ_0 such that the nanorings are on the threshold of the regime where h/e oscillations are expected.⁸

The HRS is shown in Figs. 1(b) and 1(c). Figure 1(b) shows resistance as a function of temperature and field in a resistance color contour map (RCCM). Hot and cold colors represent high and low resistances respectively. A 3D RCCM is shown in Fig. 1(c) for clarity. Note that in both plots the resistance, R , is normalized by the normal state value, R_n . Therefore the HRS increases resistance greater than fifteen times the normal state resistance. The resistance here has been measured using the current reversal method (CRM) at $I = 200$ nA. In this approach forward and reverse biases are applied to the sample and the resultant voltages are subtracted to remove parasitic

Figure 1: (Color online) (a) SEM image of sample. Top right inset: zoomed in image of the nanoring with the measurement configuration. Bottom left inset: cartoon of measurement configuration with green voltage leads and red current leads. (b) Resistance color contour map (RCCM) in B-field and temperature. (c) The same data as in (b) in 3D.

Figure 2: (Color online) (a) V vs. I scans at $T = 850mK$ and at different fields, offset for clarity, showing linear resistance higher than the normal state below the nanoring's critical current. (b) Comparison with current reversal resistance measurement (black) to the slope for $|I| < 200nA$ linear region (red). This comparison can be made at other temperatures as well.

Figure 3: (Color online) Two terminal measurements of the HRS. (a) Cartoon of different wire segments connecting to the nanoring, SEM image can be seen in Fig. 1(a). Left side shows the length of each section while the other length listed is the width. (b) Four terminal CRM resistance (red) and two terminal CRM resistance (blue) displayed simultaneously at $T = 330mK$. The lines are color coded to show the upper (solid line) and lower (dashed line) critical field of each section of leads.

thermoelectric voltages present in the low temperature measurements.

There are three distinct HRS features to be pointed out. The most obvious one is an increase of the nanoring resistance below its H_c and T_c . This resistance rises as the magnetic field decreases until it dips at a field value corresponding to an applied flux of $\Phi_0/2 = h/4e$. This is due to the LPE in the nanoring. This behavior is opposite what is expected for the LPE as it is a decrease in the transition temperature at half integer multiples of the flux quantum thereby increasing the resistance but never exceeding the normal state value.⁷ However this dip feature occurs at a magnetic field value independent of temperature and only below T_c of the nanoring. This suggests that even though there is not a zero resistance state in the nanoring, it is nevertheless phase coherent. Hence the HRS appears to be a *phase coherent resistive state*. After this LPE dip in resistance, there is an enormous resistance peak (ERP) which grows in size as temperature increases until T_c is reached. At low fields there is an apparent regime of current redistribution in the sample which makes the total current in the sample flow in the opposite direction, leading to a negative voltage drop. Finally when the field is zero, the resistance is also zero as expected in these samples.

The first test of the HRS was to measure the current-voltage (IV) characteristics at different temperatures and fields, Fig. 2(a). It is clear from Fig. 2(a) that there is linear behavior below I_c . This linear resistance at low currents is exactly the HRS exhibited in Figs. 1(b) and (c). To make this clearer R vs. B data at $850mK$ is shown in Fig. 2(b) for the CRM in black and the IV curves' slope for $|I| < 200nA$ in red. The agreement is quite good for all data except at the ERP where dR/dB is very large, so a small change in the field gives a large resistance change. Since these measurements were not taken simultaneously, it is possible that this discrepancy is due to small differences in fields produced by the magnet in separate runs.

The second check of the HRS involved the use of two-terminal measurements, which include all the wiring and electrode resistances in series with the resistance of the nanoring. This allows measurement of the H_c of the electrodes connected to the nanoring. The results are shown in Fig. 3(b). Figure 3(a) is a cartoon to understand the different critical fields present in Fig. 3(b). The exact geometry is shown in Fig. 1(a). The assumption in Fig. 3 is that the smallest width sections of the sample and electrodes have the largest critical fields.²⁰ It is clear from Fig. 3 that the HRS first appears at high fields at the critical field of the nanoring itself, which is comprised of $40nm$ wide nanowires. The ERP is clearly associated with the $100nm$ width becoming superconducting. This measurement doesn't show any sign of an HRS itself, but it does associate a few of the HRS features with the size of the leads.

Figure 4 shows the second geometry used to study the HRS. Here three different configurations can be studied: symmetric [Fig. 4(a)], local [Fig. 4(b)] and non-local [Fig. 4(c)]. The local and symmetric configurations are similar to the previous two-terminal measurements except that the nanoring is only in series with two sections of nanowire, each $\sim 1.2\mu m$ in length, similar to the geometries employed in previous works.^{12,21-23} This geometry also has the added benefits of removing the $100nm$ leads and moving the $1\mu m$ leads $> 15\mu m$ away from the nanorings to mitigate their effects.

Striking results are shown in Fig. 5. Clearly there is no HRS present in the local or symmetric measurement configurations, Figs. 5(a) and (b). However the HRS is present in the non-local configuration, Fig. 5(c). It is a little different from the HRS shown in Fig. 1, but the salient features remain. The resistance increases below the nanoring's critical field, followed by an LPE dip in resistance at half a flux quantum and a low resistance state in zero field. These data are from one sample in a single cool down of the dilution refrigerator, so the only difference is the geometry.

III. DISCUSSION AND SIMULATIONS

The literature abounds with experiments on superconducting Al nanostructures showing resistance anomalies.^{2,23} These manifest themselves as peaks in the R vs. T curves near T_c . Several models have been used to explain this excess resistance. The first used dynamic averaging of a phase slip resistance and the normal state resistance.²¹ This model was criticized in Ref.²⁴ and seems to double count the phase slip activation energy, but it can produce satisfactory fits to the zero field data

Figure 4: Second geometry employed to measure the HRS in Al nanorings. SEM image of sample with $100nm$ scale bar. This allows for three different measurement configurations to be used: (a) symmetric, (b) local and (c) non-local.

Figure 5: (Color online) 3D RCCMs of the geometry shown in Fig. 4 in the (a) symmetric, (b) local and (c) non-local configurations. Note that the color scale bar for parts (a) and (b) are the same but part (c) has its own scale bar.

in Fig. 1(b). Another potential explanation, based on experiments involving an extrinsic RF noise source,²⁵ can induce resistance anomalies but not consistently. The HRS here has been observed with and without filtering in two separate cryostats with different measurement setups.²⁶ Not to mention that the HRS is and is not observed in the same sample under the same measurement conditions with only geometrical differences. Another model is based on current path redistribution near the vertices in a superconducting network.²² This model is similar to the model that best describes the HRS, based on tilted normal metal-superconductor (NS) interfaces from Ref. 2. The model is based on having an anisotropic resistivity tensor close to a NS interface. If this interface is tilted in the proper sample geometry, a resistance higher than the normal state is possible.² However the predictions in Ref.² only show an increase $\sim 20\%$ whereas the HRS observed here is significantly higher.

Before the results of the simulations extending the results from Ref. 2 to the geometry of a ring are presented, a brief review of the physics behind the model will be provided. The model was originally proposed in Ref. 24, but not expanded upon until Ref. 2 was published. The basic idea is that due to the spatial extent of the decay of the superconducting gap near an NS interface, there exists a region of charge imbalance over the length scale of the mean free path. This charge imbalance is due to the creation and annihilation of quasiparticles and electrons in the superconducting and normal materials. This leads to an anisotropic resistance tensor parallel and perpendicular to the NS boundary. The resistance of the boundary can be simulated using Laplace's equation:

$$\frac{\partial}{\partial x} \left(\frac{1}{\rho_{xx}} \frac{\partial \phi}{\partial x} \right) + \frac{\partial}{\partial y} \left(\frac{1}{\rho_{yy}} \frac{\partial \phi}{\partial y} \right) = 0 \quad (1)$$

where ρ_{ij} are the components of the electric resistivity tensor and ϕ is the electric potential. The current density and resistance are calculated using Ohm's law. Of course there are boundary conditions due to geometrical restraints: $j_{\perp} = 0$ at the edges of the wires not connected to leads. This can only be solved numerically in most geometries of interest. To simulate the NS interface it is assumed that $\rho_s \ll \rho_n$.³ It is straightforward to compare this to the case of a completely normal ring with resistivity ρ_n .

The model in Ref. 2 was originally applied to wires with narrow and wide voltage probes with the NS interface tilted across one of the probes which lead to a resistance increase of 20%. Here it has been applied to a square ring using finite element analysis to calculate the current distribution along with the voltage measurements for symmetric, local and non-local geometries. Not

Figure 6: (Color online) Simulated resistance values measured using symmetric (blue, dot-dashed), local (red, dashed) and non-local (black, solid) configurations as a function of interface tilt angle θ measured from the vertical axis. Inset: A sample device used in simulations with interface angle $\theta = \pi/4$. Red and blue denote normal and superconducting region respectively. Inset axes are in arbitrary units.

only does the ring geometry exhibit a HRS significantly greater than the HRS found in linear case of Ref. 2, but it is extremely dependent on the measurement configuration. For simplicity all NS interfaces were assumed to be parallel. Results varied significantly depending on the placement and orientation of the NS interfaces. The configuration resulting in the highest non-local resistance measurements is shown in Fig. 6. Notice the non-local measurement clearly exhibits a HRS with $R \simeq 2R_n$ while the local and symmetric configurations show $R < R_n$ and vary little with the interface tilt. These results support the plausibility that the model from Ref. 2 can be used to explain the HRS observed experimentally here.

The origin of the tilted NS interfaces responsible for the HRS involves two effects. First, there is order parameter suppression near and in-between the vertices of a superconducting nanowire network.²⁷ The suppressed regions will have a lower critical field and therefore could form an NS interface in field in a nanoring near a vertex. Also there are natural order parameter variations in the sample due to the $\sim 25\%$ thickness variations present in the nanorings.² These two variations in the order parameter lead to normal regions, where the order parameter is driven to zero by the magnetic field. The boundaries of these regions are not perpendicular to the current and deform as the field decreases, thereby increasing the resistance. The simulations here support that the resistance increase here could be quite large. However it is infeasible at this time to extend the simulations to multiple non-parallel boundaries. This is likely the explanation for the magnitude of the HRS observed experimentally.

When the different sized electrodes become superconducting there is a massive change in the order parameter far from these nodes thereby causing massive deformation of the NS interface leading to the enormous resistance peak. There remains enough coupling between superconducting regions of the ring, such that the LPE can still be observed. Lastly, the HRS is not observed in the local and symmetric configurations because the voltage probes are too far apart. In Ref. 2 the ratio of the separation of the voltage probes to the width of the nanowire is an important parameter to determine the magnitude of the excess resistance. The two $\sim 1.2\mu\text{m}$ long nanowires in series with the nanoring in these configurations increases this ratio outside the limits one would expect to see this effect.² This is also supported by the simulations shown in Fig. 6.

The HRS data may also be better understood by looking at similar, recent data on mesoscopic superconduct-

ing Al disks.^{15–19} These data seem to suggest that the HRS only occurs when an NS boundary is present in the disk sample. The NS boundary exists in field between the disk and the measurement leads because the disk has a smaller critical field than the leads due to geometry. For example in Ref. 16 an increase in resistance is absent when the substrate is parallel to the applied field. This would prohibit (allow) the formation of an NS boundary in field because the wire and disk are the same thickness (different widths) and therefore have the same (different) critical fields in parallel (perpendicular) field. The data shown for different diameter disks in Refs. 17 and 18 agree with these statements. This picture is also consistent with data at high currents from Ref. 18 because the wires should have a lower critical current than the disk, and no NS interface can exist above this value. In Ref. 19 the linear IV characteristics at low currents and the color map look strikingly similar to the linear IV characteristics at low currents and color map in Fig. 2(a) and Fig. 1(b) respectively. These manifestations of a HRS in superconducting disks are only observed when an NS interface is set up between the disks and the electrodes. This gives further credibility to the model of tilted NS interfaces from Ref. 2.

IV. CONCLUSIONS AND FUTURE DIRECTIONS

In conclusion, a *phase coherent* high resistance state in nanorings below the superconducting transition tem-

perature has been observed. This is due to the presence of tilted NS interfaces in the nanorings producing large measured resistances. This effect can be suppressed by changing the measurement geometry and is only present when the voltage probes are extremely close together, as in the non-local configuration. It is therefore an effect unique to nanostructured superconducting rings. Understanding of this effect helps to clarify some previous unresolved questions in mesoscopic superconducting Al disks. Proper modeling of the HRS in the geometries studied here, along the lines of what has been done in Ref. 2, has provided a good qualitative understanding of the data. This work could be extended to include multiple non-parallel NS interfaces, to give a better and more quantitative understanding of the data. Also it would be interesting to see if the effect is present in ultra-clean long coherence length Al rings patterned from Al films grown on sapphire substrates. The first ever films of this quality have been produced, and could be void of the physics observed in liftoff patterned nanorings. This could also be an avenue for the observation of h/e flux quantization.

The authors would like to acknowledge A. Kamenev and K. Yu Arutyunov for useful discussions. This work has been supported by the US DOE under grant DE-FG02-02ER4600. Samples were fabricated in the Nano Fabrication Center which receives funding from the NSF as a part of the NNIN and characterized in the Characterization Facility, University of Minnesota, a member of the NSF funded Materials Research Facilities Network (www.mrfn.org) via the MRSEC program.

-
- ¹ A. M. Goldman, Int. J. of Mod. Phys. **B24**, 4081 (2010).
² K. Y. Arutyunov, D. A. Presnov, S. V. Lotkhov, A. B. Pavolotski and L. Riderer, Phys. Rev. B **59**, 6487 (1999) and references therein.
³ K. Y. Arutyunov, D. Golubev and A. Zaikin, Physics Reports **464**, 1 (2008).
⁴ M. Sahu, H. M. Bae, A. Rogachev, T. C. Wei, N. Shah, P. M. Goldbart and A. Bezryadin, Nat. Phys. **5**, 503 (2009).
⁵ Yu Chen, S. D. Snyder, A. M. Goldman, Phys. Rev. Lett. **103**, 127002 (2009). Yu Chen, Y. H. Lin, S. D. Snyder and A. M. Goldman, Phys. Rev. B **83**, 054505 (2011). M. Singh, J. Wang, M. Tian, T. E. Mallouk and M. H. W. Chan, Phys. Rev. B **83**, 220506(R) (2011).
⁶ J. E. Mooij, and Y. V. Nazarov, Nat. Phys. **2**, 169 (2006).
⁷ W. A. Little and R. D. Parks, Phys. Rev. Lett. **9**, 9 (1962).
⁸ T.-C. Wei and P. M. Goldbart, Phys. Rev. B **77** 224512 (2008).
⁹ F. Loder, A. P. Kampf, T. Kopp, J. Mannhart, C. W. Schneider and Y. S. Barash, Nature Phys. **4**, 112 (2008).
¹⁰ V. Vakaryuk, Phys. Rev. Lett. **101**, 167002 (2008).
¹¹ Y. Liu, Y. Zadorozhny, M. M. Rosario, B. Y. Rock, P. T. Carrigan and H. Wang, Science **294**, 2332 (2001).
¹² N. E. Staley and Y. Liu, PNAS **109**, 14819 (2012).
¹³ P. G. de Gennes, Comp. Ren. de l'Acad. des Sci. **292**, 279 (1981).
¹⁴ N. E. Israeloff, F. Yu, A. M. Goldman and R. Bojko, Phys. Rev. Lett. **71**, 2130 (1993).
¹⁵ Y. Terai, T. Yakabe, C. Terakura, T. Terashima, S. Yasuzuka, T. Takamasu and S. Uji, J. of Phys. and Chem. of Solids **63**, 1311 (2002).
¹⁶ K. Enomoto, T. Yamaguchi, T. Yakabe, T. Terashima, T. Konoike, M. Nishimura and S. Uji, Physica E **29** **584**, (2005).
¹⁷ A. Harada, K. Enomoto, T. Yakabe, M. Kimata, K. Hazama, H. Satsukawa, T. Terashima and S. Uji, J. of Physics: Conf. Series **150**, 022022 (2009).
¹⁸ A. Harada, K. Enomoto, T. Yakabe, M. Kimata, H. Satsukawa, K. Hazama, K. Kodama, T. Terashima and S. Uji Phys. Rev. B **81**, 174501 (2010).
¹⁹ A. Harada, K. Enomoto, Y. Takahide, M. Kimata, T. Yakabe, K. Kodama, H. Satsukawa, N. Kurita, S. Tsuchiya, T. Terashima and S. Uji, Phys. Rev. Lett. **107**, 077002 (2011).
²⁰ M. Tinkham, *Introduction to Superconductivity* (McGraw-Hill, New Yorks, 1975).
²¹ V. V. Moshchalkov, L. Gielen, G. Neuttiens, C. Van Haesendonck and Y. Bruynseraede, Phys. Rev. B **49**, 15412 (1994).
²² Ju-Jin Kim, J. Kim, H. J. Lee, S. Lee, K. W. Park and E. H. Lee, J. Phys. Condens. Matter **6**, 7055 (1994).
²³ H. Wang, M. M. Rosario, H. L. Russell and Y. Liu, Phys. Rev. B **75**, 064509 (2007).
²⁴ I. L. Landau and L. Riderer, Phys. Rev. B **56**, 6348 (1997).

- ²⁵ C. Strunk, V. Bruyndoncx, C. Van Haesendonck, V. V. Moshchalkov, Y. Bruynseraede, B. Burk, C. J. Chien and V. Chandrasekhar, *Phys. Rev. B* **53**, 11332 (1996); B. Burk, C. J. Chien, V. Chandrasekhar, C. Strunk, V. Bruyndoncx, C. V. Haesendonck, V. V. Moshchalkov and Y. Bruynseraede, *Superlattices and Microstructures* **20** 575 (1996). B. Burk, C. J. Chien, V. Chandrasekhar, C. Strunk, V. Bruyndoncx, C. V. Haesendonck, V. V. Moshchalkov and Y. Bruynseraede, *J. Appl. Phys.* **83**, 1549 (1998).
- ²⁶ The HRS was also observed in a Quantum Design Physical Property Measurement System with ^3He Insert using the internal measurement bridge. This is the same apparatus used in previous work shown in the first two papers of Ref.⁵. The data has been omitted here due to spacial constraints.
- ²⁷ H. J. Fink and V. Grunfeld, *Phys. Rev. B* **31**, 600 (1985).

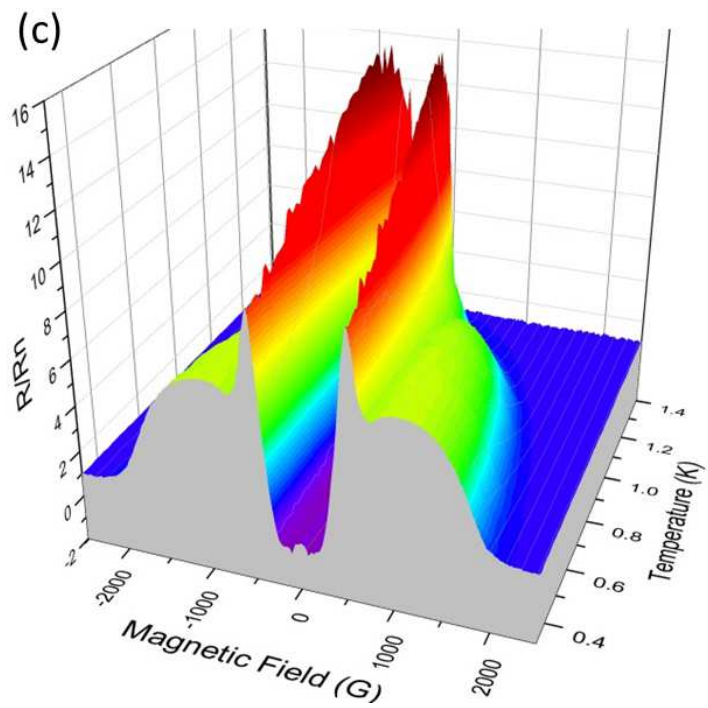
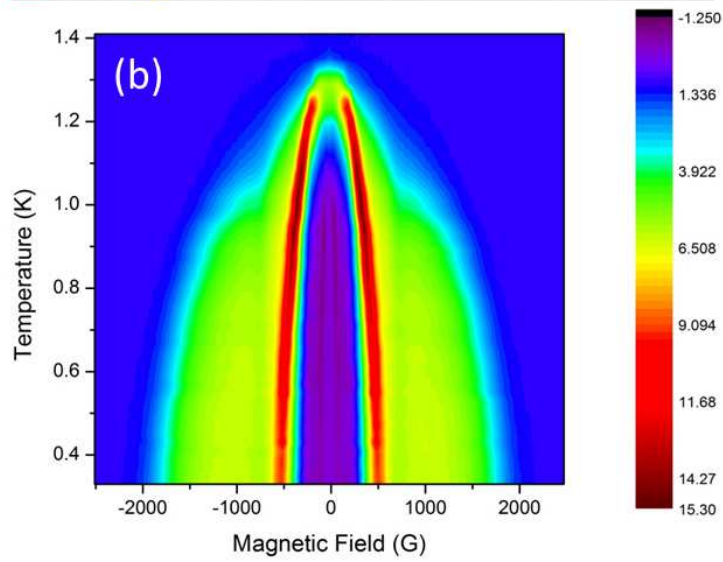
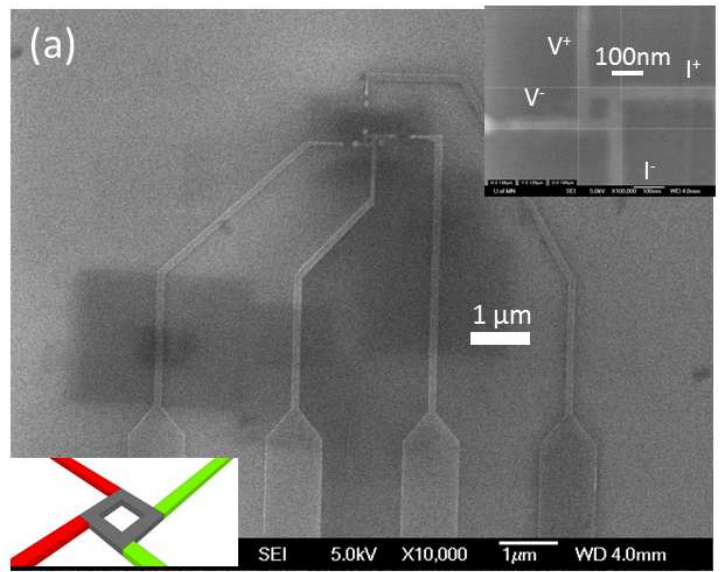


Figure 1 LV13128B 25Mar2013

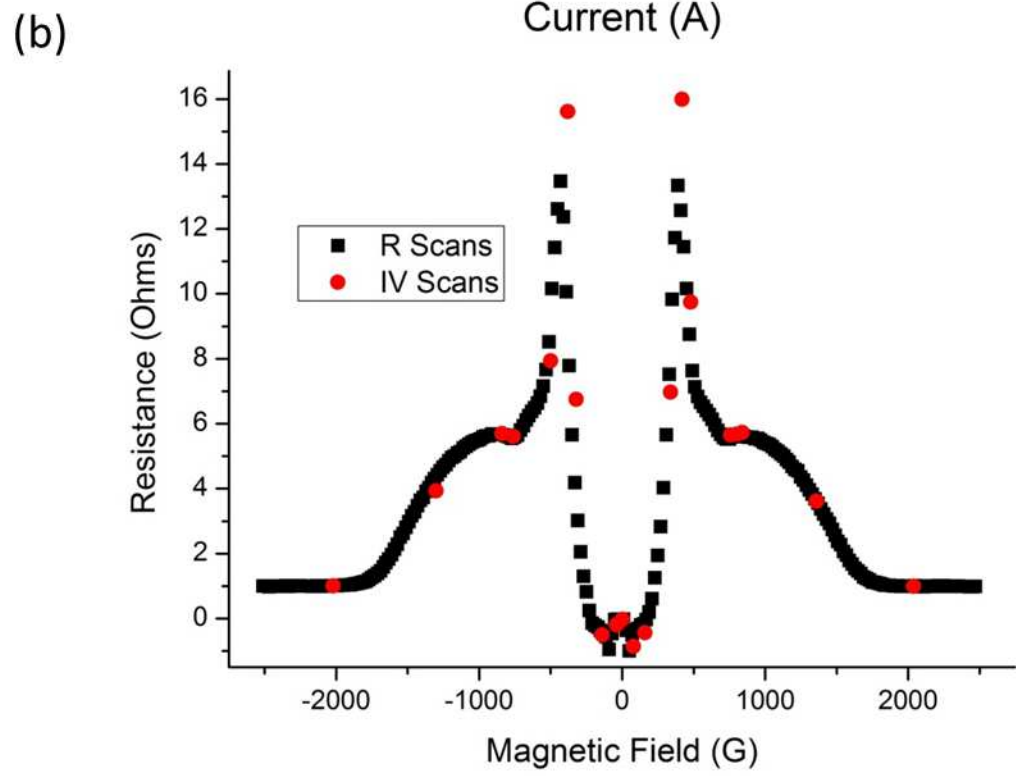
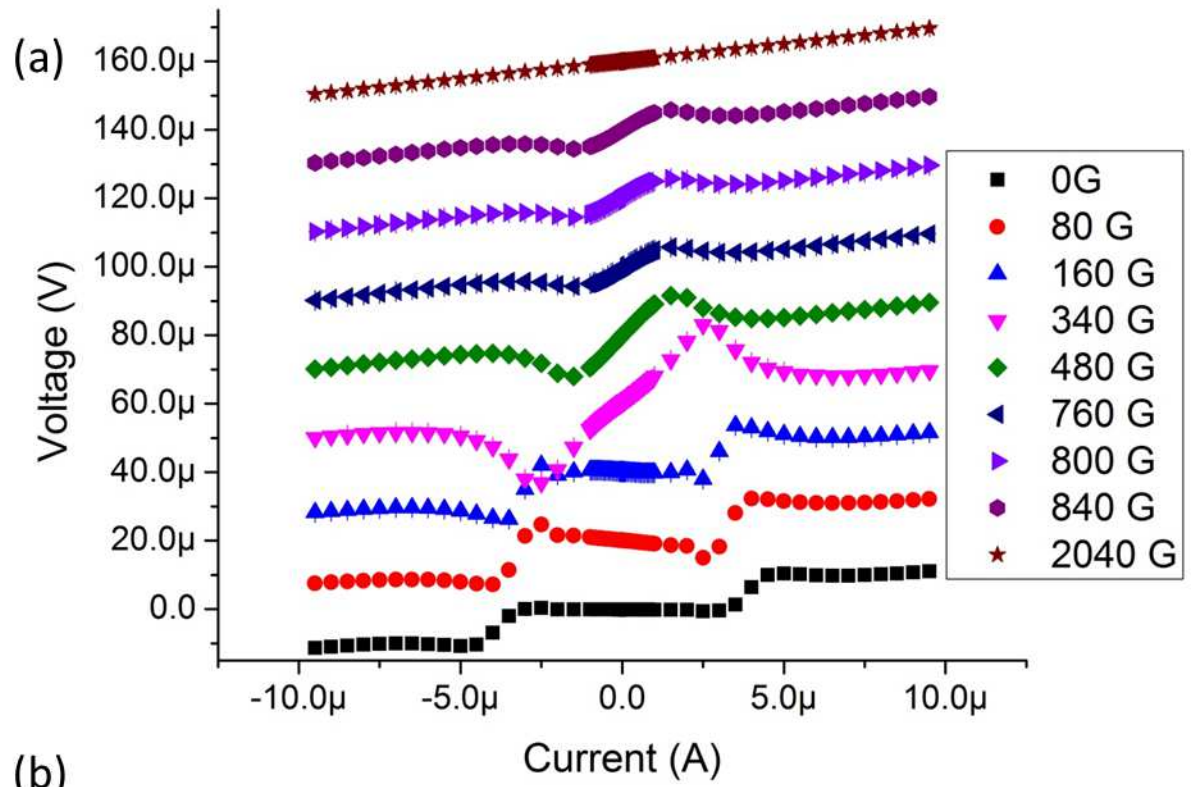


Figure 2 LV13128B 25Mar2013

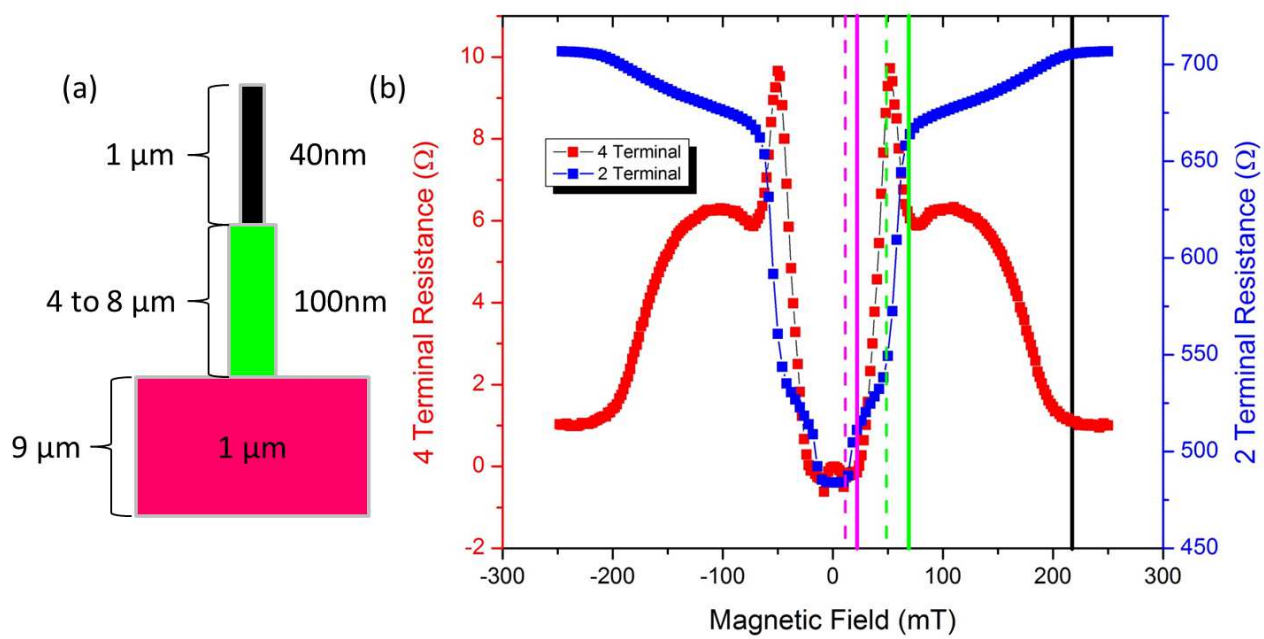


Figure 3

LV13128B

25Mar2013

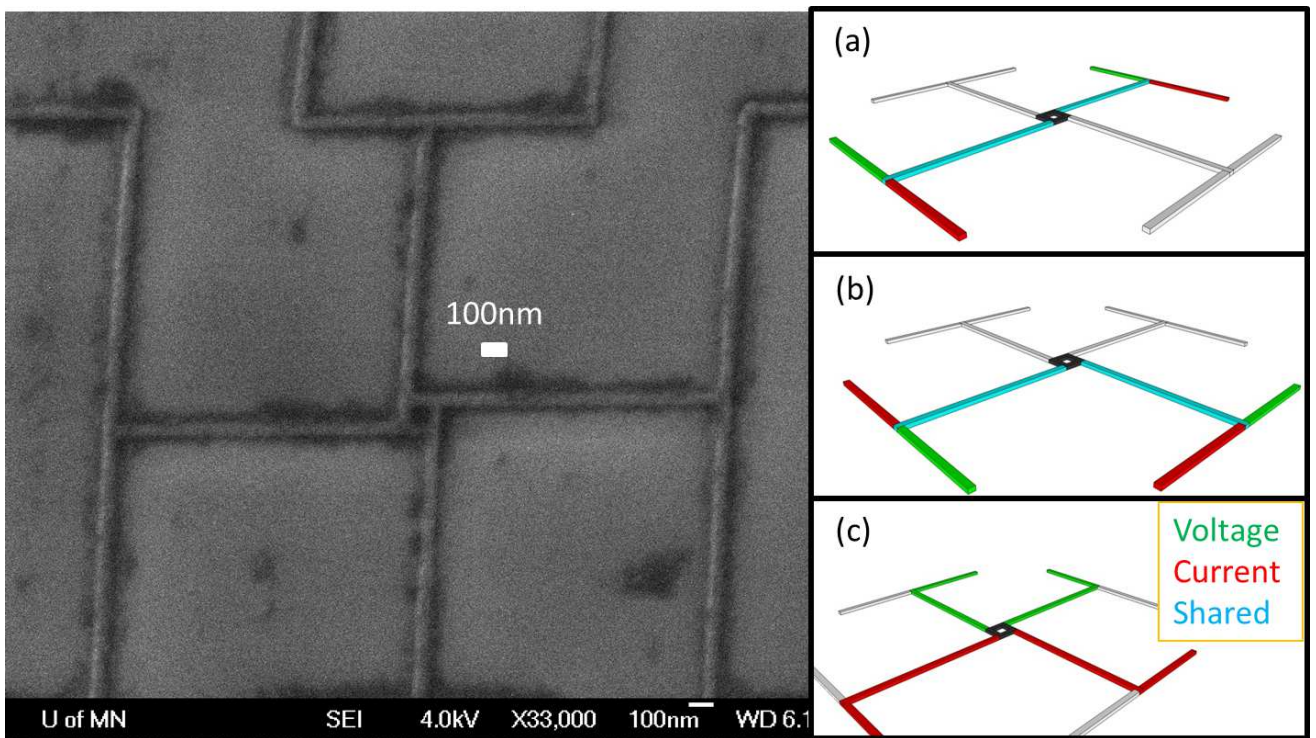


Figure 4 LV13128B 25Mar2013

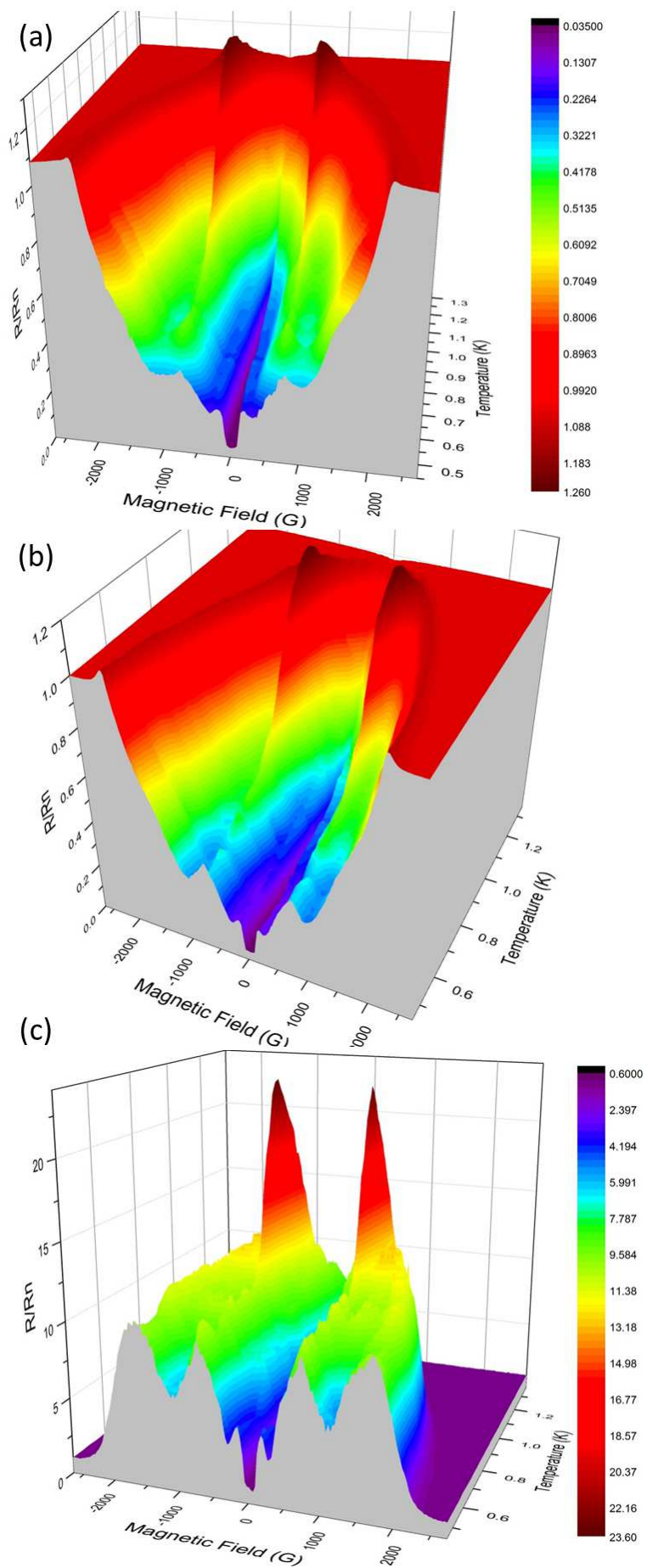


Figure 5 LV13128B 25Mar2013

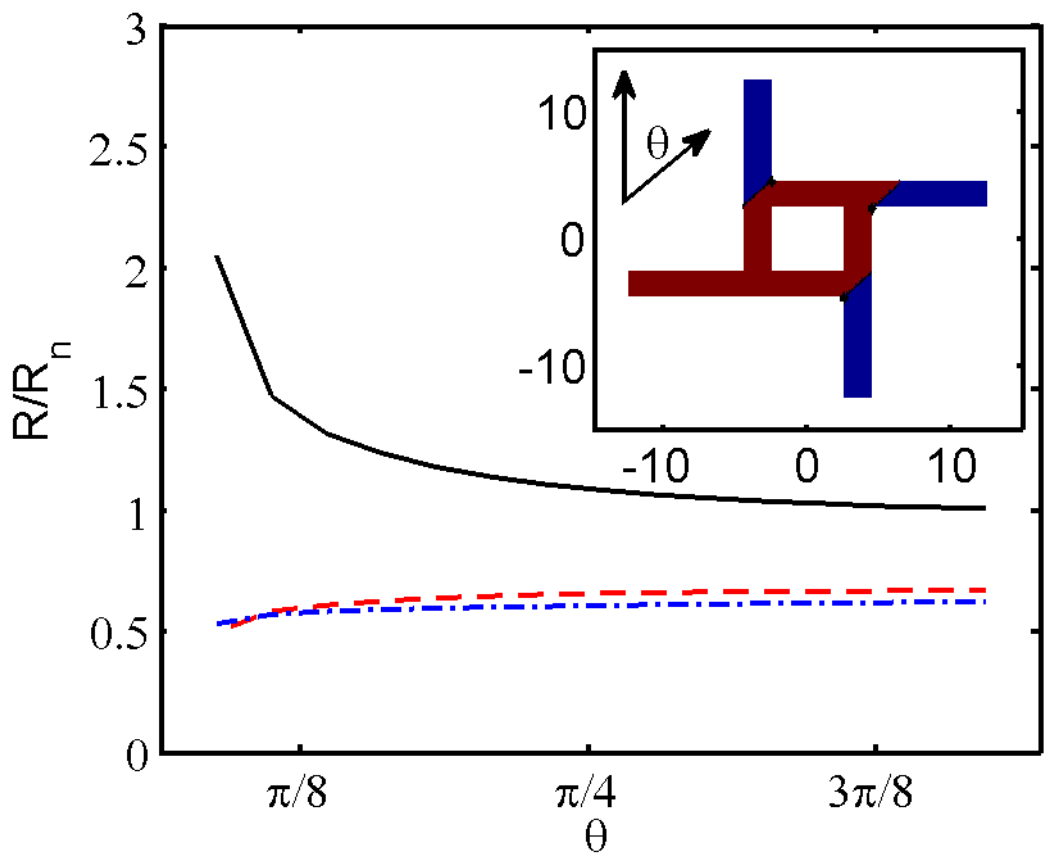


Figure 6 LV13128B 25Mar2013